

Research Paper

circPTCH1 promotes invasion and metastasis in renal cell carcinoma via regulating miR-485-5p/MMP14 axis

Huan Liu^{1*}, Guanghui Hu^{1*}, Zaoyu Wang², Qunlong Liu³, Jin Zhang⁴, Yonghui Chen⁴, Yiran Huang⁴, Wei Xue⁴✉, Yunfei Xu¹✉ and Wei Zhai⁴✉

1. Department of Urology, Shanghai Tenth People's Hospital, School of Medicine in Tongji University, Shanghai 200072, China.
2. Department of Pathology, Renji Hospital, School of Medicine in Shanghai Jiao Tong University, Shanghai 200127, China.
3. Department of Urology, Shanghai Tenth People's Hospital, Nanjing Medical University, Nanjing 210029, China.
4. Department of Urology, Renji Hospital, School of Medicine in Shanghai Jiao Tong University, Shanghai 200127, China.

*These authors contributed equally to this work.

✉ Corresponding authors: Wei Zhai, E-mail: jacky_zw2002@hotmail.com; Yunfei Xu, E-mail: xuyunfeibb@sina.com; Wei Xue, E-mail: xuwei@renji.com.

© The author(s). This is an open access article distributed under the terms of the Creative Commons Attribution License (<https://creativecommons.org/licenses/by/4.0/>). See <http://ivyspring.com/terms> for full terms and conditions.

Received: 2020.04.20; Accepted: 2020.08.18; Published: 2020.08.29

Abstract

Background: Circular RNAs (circRNAs) are a new class of non-coding RNAs (ncRNAs) that are derived from exons or introns by special selective shearing. circRNAs have been shown to play critical roles in various human cancers. However, their roles in renal cell carcinoma (RCC) and the underlying mechanisms remain largely unknown.

Methods: A novel circRNA-circPTCH1, was identified from a microarray analysis of five paired RCC tissues. Then, we validated its expression and characterization through qRT-PCR, gel electrophoresis, RNase R digestion assays and Sanger sequencing. Functional experiments were performed to determine the effect of circPTCH1 on RCC progression both *in vitro* and *in vivo*. The interactions between circPTCH1 and miR-485-5p were clarified by RNA pull-down, luciferase reporter and RNA immunoprecipitation (RIP) assays.

Results: We observed that circPTCH1 was up-regulated in RCC cell lines and tumor samples, and higher levels of circPTCH1 were significantly correlated with worse patient survival, advanced Fuhrman grade and greater risk of metastases. Elevated circPTCH1 expression led to increased migration and invasion of RCC cells both *in vitro* and *in vivo* whereas silencing circPTCH1 decreased migration and invasion and impeded the epithelial-mesenchymal transition (EMT) of RCC cells. Mechanistically, we elucidated that circPTCH1 could directly bind miR-485-5p and subsequently suppress expression of the target gene MMP14.

Conclusion: circPTCH1 promotes RCC metastasis *via* the miR-485-5p/MMP14 axis and activation of the EMT process. Targeting circPTCH1 may represent a promising therapeutic strategy for metastatic RCC.

Key words: circPTCH1, miR-485-5p, MMP14, metastasis, renal cell carcinoma

Introduction

Renal cell carcinoma (RCC) is one of the most lethal malignancies in the world and is estimated to account for approximately 4% (73,750 new cases) of newly diagnosed carcinomas and 2% (14,830 deaths) of cancer deaths in United States in 2020 [1]. Localized or early stage RCCs can be addressed with surgical treatments such as partial or radical nephrectomy,

which has a 93% five-year survival rate [2]. Although advances in imaging technologies have improved the early diagnosis rate of RCC [3], 20-30% RCC patients still present with evidence of distant metastases during their initial treatment [4]. Further, for those patients who have surgery, there is a 50% risk of developing metastases in the future [5]. Among all the

renal cancer-related deaths, more than 90% are associated with RCC metastasis [6]. Though the combination of tyrosine kinase inhibitors (TKIs) and immune checkpoint inhibitors (ICIs) has recently been recommended as a front-line therapy in metastatic RCC and has improved patient prognosis [7], most patients will still experience tumor progression and ultimately die due to drug resistance [8, 9]. Thus, it is of great clinical significance to clarify the underlying mechanisms of RCC metastasis and to identify additional prognostic biomarkers and therapeutic targets for metastatic RCC.

Circular RNAs (circRNAs) are a new class of non-coding RNAs (ncRNAs) that generated from exons or introns through special selective shearing and have a covalently closed loop structure without terminal 5' caps and 3' poly A tails [10, 11]. Due to this specific closed loop structure, circRNAs exhibit greater stability than linear RNAs under the degradation of exonuclease RNase R [12]. circRNAs were initially regarded as by-products of splicing errors when discovered many years ago. However, the wide use of high-throughput sequencing and bioinformatics analysis has demonstrated that circRNAs are endogenous, abundant, and conserved in mammalian cells which suggest that they likely have specific biological functions [13]. Recent studies have reported various physiological functions of circRNAs. They can function as protein-coding genes, sponging microRNA (miRNA/miR) to hamper mRNA translation or binding with RNA-associated proteins. For example, circFoxo3 arrests the function of CDK2 and retards cell cycle by forming a circFoxo3-p21-CDK2 triplex [14]. Circ0072391 promotes hepatoblastoma cell proliferation and apoptosis by sponging miR-503-5p [15]. A 174 amino acid (aa) novel protein encoded by circAKT3 competitively interacts with phosphorylated PDK1 to suppress the PI3K/AKT signal intensity in glioblastoma [16].

MicroRNAs, a class of short (19-22nt) ncRNAs, regulate target gene expression through targeting 3'untranslated (UTR) regions and preventing mRNA translation [17]. In recent studies, miR-485-5p has been demonstrated to act as a tumor suppressor in various cancers. For instance, miR-485-5p inhibits the development of hepatocellular carcinoma by downregulating WBP2 and blockading the Wnt/ β -catenin signaling pathway [18]. In gliomas, miR-485-5p suppresses tumor cell proliferation via directly targeting paired box 3 (PAX3) [19]. However, to our knowledge, the role of miR-485-5p in RCC has not been described to date.

In this research, we evaluated the expression profiles of circRNAs in metastatic RCC tissues and

identified a novel circRNA generated from the patched-1 (PTCH1) gene, termed circPTCH1. PTCH1 is a key component of the hedgehog (HH) signaling pathway. Mutational inactivation of PTCH1 could lead to aberrant activation of the HH pathway, which is involved in the initiation, acceleration, metastasis, and therapeutic resistance of a large number of tumors [20, 21]. Here, we found that this PTCH1-derived circRNA was significantly up-regulated in tumor tissues and cell lines using microarray analysis and qRT-PCR assays. Higher circPTCH1 expression was correlated with worse patient survival, advanced RCC Fuhrman grade and more metastases. Functional assays revealed that circPTCH1 promotes migration and invasion of RCC cells both *in vitro* and *in vivo*. Mechanistic studies implied that circPTCH1 enforces MMP14 expression by competitively binding to miR-485-5p and inducing the epithelial-mesenchymal transition (EMT) process. Therefore, our findings indicate that circPTCH1 may represent a promising therapeutic target to inhibit the invasion and metastases of RCC.

Materials and Methods

Human RCC tissue samples

The five snap-frozen tumor tissues samples used for circRNA microarray analysis were collected from metastatic RCC patients that underwent nephrectomy at the Department of Urology of Shanghai Tenth People's Hospital and Shanghai Renji Hospital. Furthermore, 39 RCC tissues and matched adjacent normal samples between January 2017 and June 2019 were collected from Shanghai Tenth People's Hospital and Renji Hospital for validation. All RCC cases were confirmed by a senior pathologist from each hospital. The demographic data, pathologic characterization and representative pathological figures of RCC samples are listed in Table S1. The use of all tissue specimens was evaluated and approved by the Ethical Committees of Shanghai Tenth People's Hospital affiliated Tongji University, and Renji Hospital affiliated School of Medicine in Shanghai Jiaotong University. Written informed consent was obtained from every patient.

Microarray analysis

Total RNA from each sample was quantified using a NanoDrop ND-1000. The sample preparation and microarray hybridization were performed based on Arraystar's standard protocols (KANGCHEN Biotech, Shanghai, China). In brief, total RNA was digested with RNase R (Epicentre, Inc.) to remove linear RNAs and enrich for circular RNAs. Then, the enriched circRNAs were amplified and transcribed into fluorescent cRNA using a random priming

method (Arraystar Super RNA Labeling Kit; Arraystar). The labeled circRNAs were hybridized onto the Arraystar Human circRNA Array V2 (8×15K, Arraystar). Next, the slides were washed and the arrays were scanned using an Agilent Scanner G2505C. Agilent Feature Extraction software (version 11.0.1.1) was applied to analyze the acquired array images. Quantile normalization and subsequent data processing were performed using the R software limma package. Differentially expressed circRNAs with statistical significance between two groups were identified through Volcano Plot filtering. Significantly differentially expressed circRNAs were then further filtered through analysis of Fold Change. Hierarchical Clustering was performed to highlight distinguishable circRNAs expression patterns among samples.

Bioinformatics analyses

The sequence of circPTCH1 was acquired from circBase. To predict the potential miRNAs binding with circPTCH1, we used three online analysis tools: Circular RNA Interactome, circAtlas 2.0 and starBase v2.0. The expression of miRNAs and mRNAs candidates was evaluated using The Cancer Genome Atlas Program (TCGA) Kidney Clear Cell Carcinoma (KIRC) database, or the UALCAN database [22]. The downstream target genes of miR-485-5p were predicted using TargetScan, starBase v2.0, miRDB, miWALK and miDIP. The websites linking to the above online databases are listed in Table S2.

Cell lines and cultivate

Human RCC cell lines ACHN, OS-RC-2, A498, 786-O and normal kidney tubular epithelial cell HK-2 were purchased from the Cell Bank of Chinese Academy of Sciences (Shanghai, China). HK-2 was cultivated in Keratinocyte Medium (ScienCell, San Diego, USA) plus 1% Keratinocyte Growth Supplement (ScienCell, San Diego, USA) and the other RCC cells and HEK293T were cultured in Gibco Dulbecco's Modified Eagle's Medium with 10% Fetal Bovine Serum (FBS, Hyclone, Utah, USA). All media contained 1% Gibco Penicillin/Streptomycin (New York, USA). All cells were cultured in the same humidified atmosphere (37 °C with 5% CO₂).

RNA extraction, reverse transcription, and quantitative real-time PCR analysis (qRT-PCR)

Total RNA was extracted from cells or human tissues using Trizol reagent as directed by the manufacturer (Invitrogen, CA, USA). To isolate RNA from the nuclear and cytoplasmic fractions, a PARIS™ Kit was used (Invitrogen, CA, USA). A Nanodrop

2000 spectrophotometer was used to measure RNA purity and concentration (Thermo Fisher Scientific, Inc., Waltham, MA, USA). Reverse transcription was performed to synthesize cDNA using the PrimeScript RT reagent kit (TaKaRa, Japan). qRT-PCR was conducted using a SYBR Green qPCR Kit (Takara, Japan) and the ABI Prism 7500 Detection System (Applied Biosystems, USA). The expression of circRNAs, mRNAs and miRNAs were calculated normalized to internal control GAPDH or U6 using the 2^{-ΔΔCt} method. The detailed primer sequences are listed in Table S3.

Western blot analysis

Cells were lysed on ice using RIPA buffer (Beyotime, Shanghai, China) containing protease inhibitors. Equal amounts (30 μg) of protein samples was loaded onto a 10% SDS-PAGE gel and then transferred to nitrocellulose or polyvinylidene fluoride membranes. The membranes were blocked in 5% skim milk and then incubated overnight at 4 °C with primary antibodies as follow: MMP14 (1:1000, Abclonal, China), E-cadherin (1:1000, Abclonal, China), N-cadherin (1:1000, Abclonal, China), Vimentin (1:1000, Abclonal, China), GAPDH (1:5000, Abcam, UK). Next, the membranes were incubated with secondary mouse or rabbit antibodies for 1 h at room temperature. After 3 washes with PBST, the fluorescence was measured using an Odyssey scanner (LI-COR, Biosciences, NE, USA).

Immunofluorescence

After various treatments, cells were fixed with 4% paraformaldehyde, permeabilized in 0.3% Triton X-100, and then blocked in 5% goat serum. Later, cells were incubated overnight at 4 °C with antibody against E-cadherin (1:200, Abclonal, China) or N-cadherin (1:200, Abclonal, China). Secondary fluorescent antibody conjugated Alexa Fluor 488/594 was added and incubated at room temperature for 1 h. DAPI was used for nuclear counterstaining. Images were captured using a confocal microscope (Leica Microsystems, Buffalo Grove, USA).

Wound healing assays

After various treatments, cells were seeded in triplicate into 6-well plates and, after reaching 80-90% confluency, a wound was made using a 200 μL pipette tip on the cell monolayer. Culture media was then replaced with 2% FBS DMEM. Next, cells were incubated to allow to heal for additional 24 h and then photographed via microscopy (Leica Microsystems, Mannheim, Germany).

Transwell assays

Transwell chambers (Corning, MA, USA) with 8 μm pore size polycarbonate filters were used to evaluate the migration and invasion abilities of RCC cells. 5×10^4 cells in serum-free media were seeded in the upper chamber pre-covered with or without Matrigel (Corning, BD356230, USA), and 600 μL 10% FBS culture media was added to the lower chamber. After incubation, cells in the upper surface of the filters were gently removed using a cotton swab. Then, the cells that migrated or invaded to the lower surface of the filter were fixed in 95% ethanol for 15 min and stained with 0.1% crystal violet solution for 20 min. Cell numbers were measured and averaged across five randomly selected fields under a microscope (Leica Microsystems, Mannheim, Germany).

RNase R and Actinomycin D treatment assay

According to the protocols previously described [23, 24], RNA was incubated with RNase (3 units per μg , Genesee Biotech, Guangzhou, China) for 30 min and RCC cells were exposed to 2 $\mu\text{g}/\text{mL}$ Actinomycin D (HY-17559, Medchemexpress, Monmouth Junction, NJ, USA) for 8, 16, or 24 h. Then, the expression of circPTCH1 and PTCH1 were detected by qRT-PCR.

Fluorescence *in situ* hybridization (FISH)

Cy3-labeled probe specific to circPTCH1 was purchased from Ribobio (Guangzhou, China). Cell nuclei were stained with DAPI. The FISH experiment was performed using the Fluorescence *in situ* hybridization kit (C10910, Ribobio, Guangzhou, China) following the manufacturer instructions. Images were acquired using a microscope (Leica Microsystems, Mannheim, Germany).

Cells transfection

Two small-interfering RNAs (siRNAs) specifically targeting circPTCH1 were designed and generated by IBSBIO Biotech (Shanghai, China). MiRNA negative control (mi-NC), miR-485-5p mimics and inhibitors were purchased from Ribobio (Guangzhou, China). Transient transfection of these reagents was conducted using Lipofectamine 3000 (Thermo Fisher Scientific). For circRNA over-expression, the circPTCH1 overexpressed plasmid was synthesized by BioLink (Shanghai, China). Then, we transfected the plasmids into HEK293T cells to package lentivirus using a Lentivirus-Packaging kit (BioLink, Shanghai, China). After 24h, lentivirus supernatants were collected and used to infect cells.

RNA pull-down assay

The biotin-labeled circPTCH1 probe was

synthesized by BIOFAVOR Biotech (Wuhan, China). In brief, 2×10^7 cells were harvested and lysed in 100 μL RIP lysis buffer on ice, then incubated with a high-affinity biotin-labeled probe for 1 h at room temperature. Next, the suspension and streptavidin magnetic beads were mixed for 1 h at room temperature. The beads were washed using RIP wash buffer and the RNAs pulled down on the beads were extracted using Trizol and analyzed by qRT-PCR assay and gel electrophoresis.

Luciferase reporter analysis

The potential binding sites of miR-485-5p and circPTCH1 or MMP14 were obtained from circAtlas and TargetScan, and the sequences were mutated and cloned into a psiCHECK-2 vector (Promega Corporation, WI, USA). RCC cells were seeded in 12-well plates and co-transfected with the luciferase reporter vector (circPTCH1-WT/Mut or MMP14-WT/Mut) and miR-485-5p mimics or NC. After 48 h of transfection, the relative luciferase activity was measured by Dual Luciferase Assay System according to the manufacturer's protocol (Promega, Massachusetts, USA).

RNA immunoprecipitation (RIP) assay

The RIP assay was performed using an EZ-Magna RIP kit (Millipore, MA, USA) per the manufacturer's instructions. Briefly, RCC cells were harvested and lysed in RIP lysis buffer, and then incubated with magnetic beads coated with anti-Ago2 or anti-IgG antibody (Santa Cruz). Next, the immunoprecipitated RNAs were extracted as described above and detected by qRT-PCR.

Orthotopic tumor implantation in nude mice

For *in vivo* tumor studies, 4-6 weeks old Balb/c nude mice were purchased from Shanghai Sipper-BK Laboratory Animal Company (Shanghai, China). The mice were kept in a specific pathogen-free environment and all operations on mice were conducted following protocols approved by the Animal Research Ethics Committee of the Shanghai Tenth People's Hospital, Tongji University. OS-RC-2 cell line stably expressing firefly luciferase cell line (OS-RC-2-luci) was constructed as previously described [9]. Each mouse was injected with 1×10^6 OS-RC-2-luci cells (vector or OE-circPTCH1) into the left subrenal capsule (1:2 mixed with Matrigel before injection). To detect the role of miR-485-5p *in vivo*, the miR-485-5p agomir or NC (Ribobio, Guangzhou, China) were injected continuously into the tail vein for 2 weeks according to prior publications and the manufacturer's recommendations [25]. Tumor progress and metastasis were observed using the IVIS imaging system (Calipers, Hopkinton, USA). After 6

weeks, all mice were sacrificed and the tumors and metastatic tissues were harvested for analysis.

Immunohistochemistry (IHC)

IHC was conducted on tumor samples from xenograft mice following the methods described previously [26]. The tumor specimens were fixed in formalin, embedded in paraffin and then cut into 4 μ m slices. After dewaxing, rehydration, and antigen retrieval, these slides were incubated with specific primary antibodies against MMP14, E-cadherin, or N-cadherin (Abclonal, Wuhan, China). Images were photographed using a microscope (Leica Microsystems, Mannheim, Germany).

Statistical analysis

Statistical analyses were performed using the GraphPad Prism 8 (GraphPad Software, San Diego, CA, USA) and SPSS 19.0 software (SPSS, Inc., Chicago, USA). All data were presented as mean \pm standard deviation (SD) from three independent experiments. Statistical significance was analyzed using Student's *t*-tests. The Kaplan-Meier method was applied to assess survival curves, and differences were measured by a log-rank test. The correlations between circPTCH1, miR-485-5p and MMP14 were evaluated using Pearson's correlation coefficient. All data were considered statistically significant at a *p*-value < 0.05.

Results

Identification of circPTCH1 from microarray analysis and characterization in RCC cells

A microarray-based circRNA expression profile analysis was conducted on five metastatic RCC tissues and paired adjacent normal specimens. In total, 9,591 distinct circRNAs were detected (Figure S1A). circRNAs with | fold change (FC) | \geq 2 and *p*-values < 0.05 were considered to be significantly differentially expressed. The significantly dysregulated circRNAs were presented in a volcano and clustered heat map (Figure S1B-C).

To identify circRNAs that promote metastasis in RCC, we focused on the top five up-regulated circRNAs according to FC (Table S4). The expression of those circRNAs was examined in both RCC cell lines and 39 paired tumor samples by qRT-PCR analysis. Among them, only hsa_circ_0139402 was found to be highly expressed in all RCC cell lines compared with HK-2 (Figure S2 and Figure 1A), which was consistent with the results of our microarray analysis. Further, hsa_circ_0139402 was also expressed at higher levels in tumor specimens compared with adjacent normal tissues (Figure 1B). Higher circPTCH1 expression was also correlated

with worse RCC patient survival (Figure 1C). Because the OS-RC-2 and A498 cell lines had higher expression of circPTCH1, we selected these two cells for further studies.

Hsa_circ_0139402 consists of exon 13 and 14 of PTCH1 (522 bp) and its head-to-tail splicing structure was confirmed by Sanger sequencing (Figure 1D). Since hsa_circ_0139402 was derived from the host gene PTCH1 (Gene ID: 5727), we named it circPTCH1. Divergent and convergent primers were designed to separately detect the expression of circPTCH1 and linear PTCH1 using gel electrophoresis. We found that circPTCH1 could only be amplified in cDNA but not in genomic DNA (gDNA) using divergent primers while PTCH1 was amplified in both cDNA and gDNA by convergent primers (Figure 1E). To evaluate the stability of circPTCH1, we treated the RNA from OS-RC-2 and A498 cells with RNase R and found that circPTCH1 was more stable to RNase R digestion whereas linear PTCH1 was clearly digested following RNase R treatment (Figure 1F). Similar results were observed using Actinomycin D (inhibitor of transcription) assay. As shown in Figure 1G, the half-life of the circPTCH1 transcript exceeded 24 h while linear PTCH1 transcription was blocked obviously. To investigate the subcellular localization of circPTCH1, we measured the expression of circPTCH1 in nuclear and cytoplasmic fractions of A498 and OS-RC-2 cells using qRT-PCR analysis and found that circPTCH1 was predominately distributed in the cytoplasm (Figure 1H). FISH assay also indicated that circPTCH1 was located predominantly in the cytoplasm (Figure 1I).

circPTCH1 enhances the migration and invasion of RCC cells *in vitro*

To inhibit the expression of circPTCH1 in RCC cells, two siRNAs specifically targeting the junction sites of circPTCH1 were transfected into OS-RC-2 and A498 cells. Subsequent qRT-PCR results showed that both siRNAs (si-circ-1 and si-circ-2) decreased circPTCH1 expression but did not affect the PTCH1 mRNA levels (Figure 2A). Si-circ-2 was selected for use in latter assays as it has a better suppressive efficiency. Wound healing assays indicated that silencing circPTCH1 significantly suppressed cell migration in both OS-RC-2 and A498 cells (Figure 2B-C). Further, transwell assays also revealed that the migration and invasion of OS-RC-2 and A498 cells were blocked after inhibition of circPTCH1 (Figure 2D-E). Additionally, we upregulated circPTCH1 by transfecting the circPTCH1 overexpressed plasmids into RCC cells (Figure 2F). Conversely, the healing ability of A498 and OS-RC-2 cells was obviously enhanced (Figure 2G-H) and the migration and

invasion of RCC cells were significantly increased in transwell migration and matrigel invasion assays (Figure 2I-J).

Next, we explored the correlations between circPTCH1 expression and special clinicopathological

features in the set of 39 clinical RCC cases. As presented in Table 1, circPTCH1 expression was significantly positively related with RCC tumor Fuhrman grade and metastasis ($p < 0.05$).

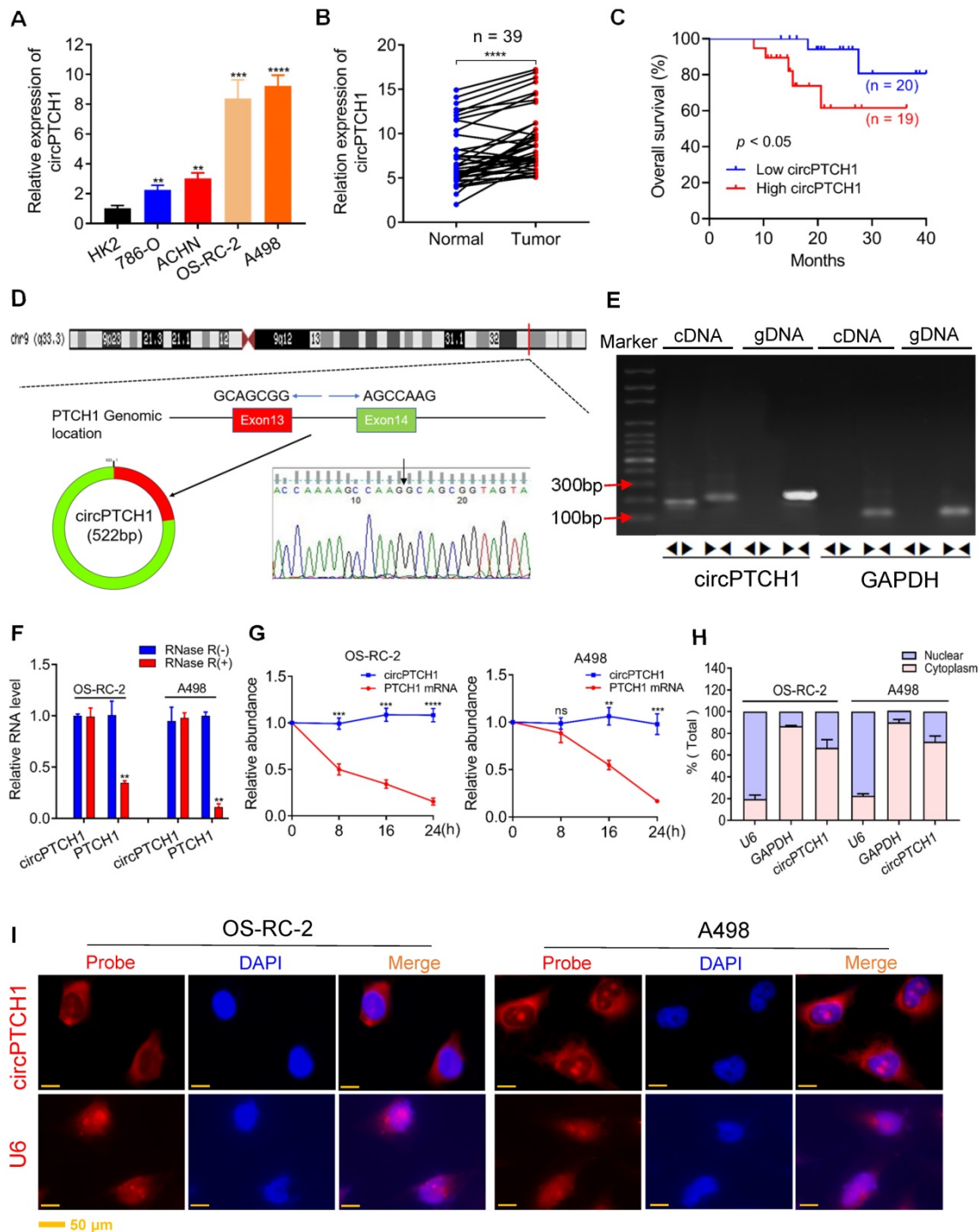


Figure 1. The expression and characterization of circPTCH1 in RCC cells. **A.** Relative expression of circPTCH1 in human normal kidney tubular epithelial cell HK-2 and RCC cell lines (786-O, ACHN, OS-RC-2 and A498). **B.** Relative expression of circPTCH1 detected by qRT-PCR in 39 paired ccRCC tissues compared with adjacent normal tissues. **C.** Kaplan-Meier’s survival analysis indicated that circPTCH1 expression was correlated with worse patient prognosis. **D.** Schematic illustration shows that circPTCH1 formed from exon 13 and 14 of PTCH1 and the existence of circPTCH1 was validated by Sanger sequencing. Black arrow represents the back-splicing site of circPTCH1. **E.** The existence of circPTCH1 was validated by qRT-PCR and Gel electrophoresis. Divergent primers could amplify circPTCH1 in cDNA but not gDNA. GAPDH was used as negative control. **F-G.** The qRT-PCR results showed circPTCH1 was more stable than linear PTCH1 after treatment with RNase R or Actinomycin D. **H.** qRT-PCR analysis of circPTCH1 was conducted in nuclear and cytoplasmic fractions of OS-RC-2 and A498 cells. **I.** FISH indicated that circPTCH1 was predominantly located in cytoplasm of OS-RC-2 and A498 cells. Nuclei were stained with DAPI and circPTCH1 was labeled with Cy3. U6 probe was applied as negative control. Scale bar, 50 μ m. * $p < 0.05$, ** $p < 0.01$, *** $p < 0.001$, **** $p < 0.0001$. cDNA: complementary DNA; gDNA: genomic DNA; FISH: fluorescence *in situ* hybridization. RCC: renal cell carcinoma.

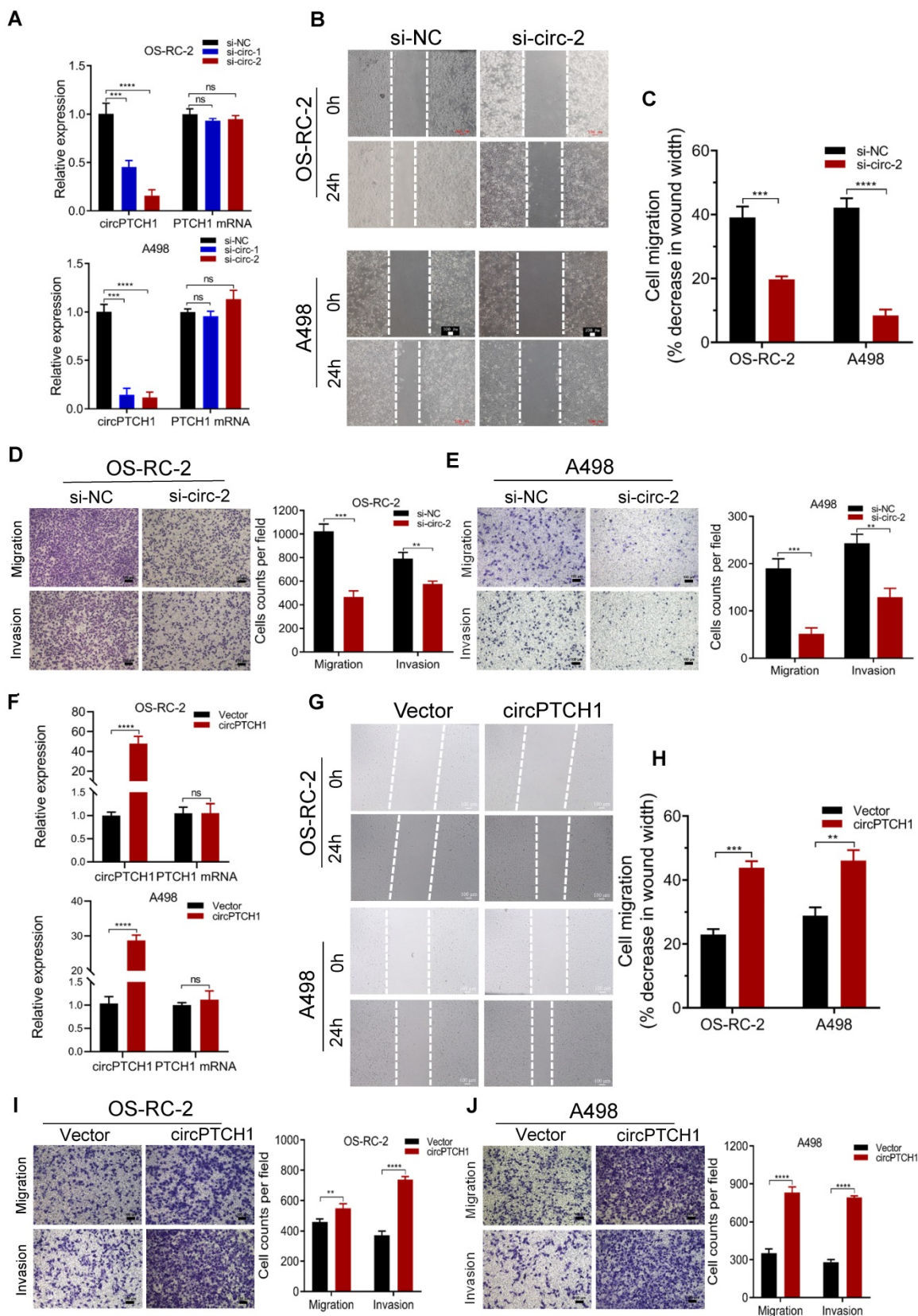


Figure 2. circPTCH1 enhances the migration and invasion of RCC cells in vitro. **A.** Two specific siRNAs (si-circ-1 and si-circ-2) were designed to interfere circPTCH1 expression and the suppressive efficacy on circPTCH1 and PTCH1 mRNA was measured by qRT-PCR. **B-C.** Cell migration capability of OS-RC-2 and A498 transfected with si-circ-2 or si-NC was assessed by wound healing assay. **D-E.** Cell migration and invasion abilities of OS-RC-2 and A498 transfected with si-circ-2 or si-NC was assessed by transwell migration and matrigel invasion assays. **F.** The expression of circPTCH1 and PTCH1 mRNA in OS-RC-2 and A498 cells transfected with circPTCH1 or vector plasmids were detected by qRT-PCR. **G-H.** Cell migration capability of OS-RC-2 and A498 transfected with circPTCH1 or vector was assessed by wound healing assay. **I-J.** Cell migration and invasion abilities of OS-RC-2 and A498 transfected with circPTCH1 or vector were assessed by transwell migration and matrigel invasion assays. Scale bar, 100 μ m. * p < 0.05, ** p < 0.01, *** p < 0.001, **** p < 0.0001. ns: none significance; NC: negative control; RCC: renal cell carcinoma.

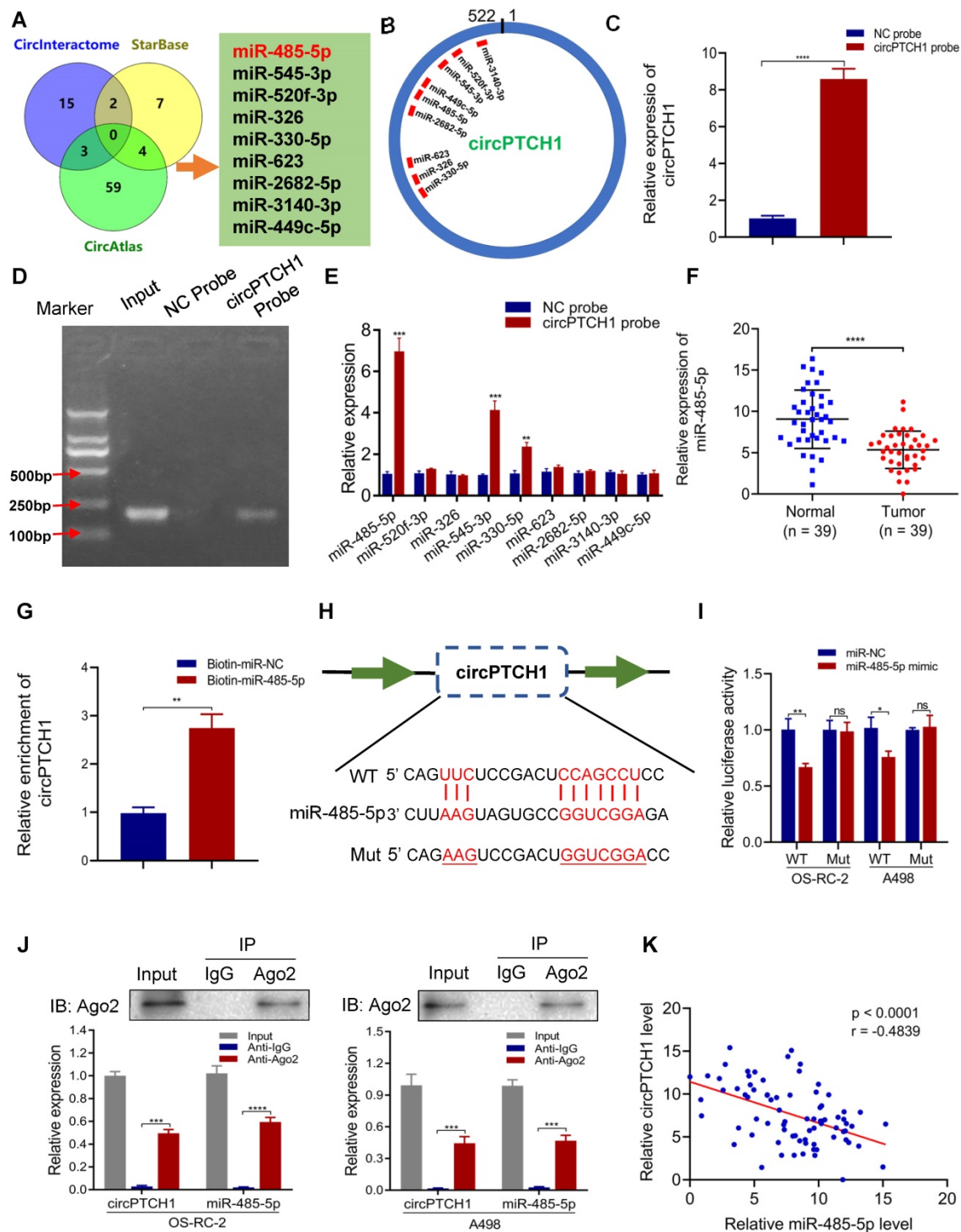


Figure 3. circPTCH1 acts as a sponge of miR-485-5p. **A.** Nine potential miRNAs absorbed by circPTCH1 were predicted through CircInteractome, Starbase and CircAtlas. **B.** Schematic model revealed the putative binding sites of nine miRNA candidates with circPTCH1. **C-D.** The efficiency of circPTCH1 probe was validated by qRT-PCR and gel electrophoresis. **E.** Relative expression of miRNAs enriched by circPTCH1 probe in HEK293T cells lysates was detected by qRT-PCR. **F.** The expression of miR-485-5p in 39 paired RCC tumor samples and adjacent normal tissues. **G.** Relative circPTCH1 level in HEK293T cells lysates captured by biotin-labeled miR-485-5p or NC was detected by qRT-PCR. **H-I.** Relative luciferase activities in RCC cells co-transfected with circPTCH1-WT or circPTCH1-Mut and miR-485-5p mimics or NC. **J.** RIP assay was utilized to verify the association between circPTCH1 and miR-485-5p. Top, IP efficiency of Ago2-antibody shown in western blotting. Bottom, relative RNA levels compared with input. IgG served as a negative control. **K.** circPTCH1 expression was inversely correlated with miR-485-5p level using Pearson correlation analysis in RCC samples. * $p < 0.05$, ** $p < 0.01$, *** $p < 0.001$, **** $p < 0.0001$. ns: none significance; NC: negative control; Ago2: Argonaute-2; WT: wild type; Mut: mutant type; RCC: renal cell carcinoma; IP: Immunoprecipitation.

In summary, the results from *in vitro* studies and clinical analyses indicate that circPTCH1 is significantly up-regulated in RCC tissues and cell

lines and functions as an oncogene by promoting migration and invasion in RCC cells.

circPTCH1 acts as a sponge of miR-485-5p in RCC cells

It has been reported that circRNAs, which mainly located in the cytoplasm, always function as a sponge of miRNAs [27]. Thus, we predicted the potential target miRNAs of circPTCH1 using three online prediction tools: Circular RNA Interactome, circAtlas and starBase v2.0. In total, 90 miRNAs emerged as potential targets, but none were predicted across all three databases. Therefore, we narrowed the candidates to nine miRNAs (miR-485-5p, miR-545-3p, miR-520f-3p, miR-326, miR-330-5p, miR-623, miR-2682-5p, miR-3140-3p and miR-449c-5p) that were predicted across two of the three prediction tools (Figure 3A). The putative binding sites of circPTCH1 are shown in Figure 3B. RNA-pull down assay was performed to evaluate the interactions between these miRNAs and circPTCH1. Biotin-labelled circPTCH1 probe was synthesized by BIOFAVOR Biotech (Wuhan, China) and the efficiency was validated by qRT-PCR and gel electrophoresis (Figure 3C-D). Among these nine candidates, miR-485-5p, miR-545-3p, and miR-330-5p were abundantly pulled down by the circPTCH1 probe compared with the NC probe, and miR-485-5p was the most enriched (Figure 3E). Next, we investigated the expression of these miRNAs in RCC based on TCGA KIRC database. The results showed that only miR-485-5p was significantly down-regulated in RCC tissues (Figure S3), which implied that miR-485-5p may play the same anti-tumor role in RCC as previously reported in hepatocellular carcinoma and lung cancer [28, 29]. To further validate this result, we measured miR-485-5p levels in our 39 paired RCC samples using qRT-PCR analysis. Indeed, miR-485-5p was significantly overexpressed in adjacent normal renal tissues relative to tumor specimens (Figure 3F). We next used biotin-labeled miR-485-5p mimics and NC to capture circPTCH1 and found that more circPTCH1 was captured by miR-485-5p mimics, further supporting the hypothesis that circPTCH1 acts as a sponge of miR-485-5p (Figure 3G).

To elucidate the interaction between circPTCH1 and miR-485-5p, we inserted the luciferase reporter with wild or mutant-type sequences that were predicted to be potential binding sites for circPTCH1 and miR-485-5p (Figure 3H). The relative luciferase activity was decreased by miR-485-5p mimics in OS-RC-2 and A498 cells transfected with wild-type constructs while no significant difference was observed in the mutant group (Figure 3I). Furthermore, we found that circPTCH1 and miR-485-5p could both be enriched by beads coated with

anti-Ago2 compared with anti-IgG (Figure 3J). Additionally, as shown in Figure 3K, circPTCH1 expression was inversely associated with miR-485-5p levels in our clinical samples.

Taken together, the above results implied that circPTCH1 serves as a competing endogenous RNA (ceRNA) via sponging miR-485-5p.

miR-485-5p suppresses the migration and invasion of RCC cells through targeting MMP14

To evaluate the role of miR-485-5p in RCC, we transfected miR-485-5p mimics, inhibitors, or NC into OS-RC-2 and A498 cells. These gain- and loss-of-function experiments showed that upregulation of miR-485-5p significantly inhibited the migration and invasion of OS-RC-2 and A498 cells, and silencing miR-485-5p enhanced the migration and invasion of RCC cells (Figure 4A-D).

To unravel the downstream target gene of miR-485-5p, we used a set of online prediction tools: TargetScan, starBase v2.0, miRDB, miWALK and miDIP. Initially, 39 candidates were identified across all prediction tools (Figure 4E). Then, we detected their expression in RCC tissues and found 6 (MMP14, ZNF384, BAZ2A, EFNA1, MEF2D and MAX) were significantly up-regulated in tumor tissues based on TCGA KIRC database and the Clinical Proteomic Tumor Analysis Consortium (CPTAC) ccRCC Dataset [30] (Figure S4A-B). Among those 6, we concentrated on MMP14 as it was the most aberrantly expressed (Figure S4A-B), and has been well-known relevant with metastasis of various tumors. Our clinical specimens also demonstrated that MMP14 was significantly differentially expressed in RCC samples (Figure 4F). Additionally, it has been reported that miR-485-5p suppresses migration and invasion of glioma cells through modulating the target gene MMP14 [31]. To validate the interaction between miR-485-5p and MMP14, we inserted the luciferase reporter with wild-type MMP14 3'-UTR or mutant sequences (Figure 4G). As shown in Figure 4H, the relative luciferase activity was efficiently decreased by miR-485-5p mimics in RCC cells transfected with wild-type constructs, while there was no significant difference observed in the MMP14 mutant group. Meanwhile, we observed a negative correlation between miR-485-5p and MMP14 expression in RCC samples (Figure 4I) and western blot showed that the protein level of MMP14 was altered following transfection with miR-485-5p inhibitors or mimics (Figure 4J), which also demonstrated that MMP14 is targeted by miR-485-5p.

We also assessed the prognostic value of miR-485-5p and MMP14 using the TCGA cohort. As shown in Figure S4C, high MMP14 expression correlated with worse patient survival ($p = 0.018$), consistent with our prior experiments. However, there was no apparent association between miR-485-5p and survival of RCC patients ($p = 0.89$) (Figure S4D). The relationship between expression of MMP14 or miR-485-5p and clinical features of RCC was also evaluated using TCGA data. As shown in Table S5, we found that MMP14 expression was significantly correlated with RCC tumor T stage ($p = 0.014$), grade ($p = 0.044$), and pathologic stage ($p = 0.025$). And miR-485-5p was observed significantly associated with RCC tumor T stage ($p = 0.036$). These results reveal that MMP14 or miR-485-5p may have potential as a novel prognostic indicator of RCC.

Collectively, these results demonstrate that miR-485-5p could significantly suppress migration and invasion of RCC through targeting MMP14.

circPTCH1 facilitates migration, invasion, and EMT of RCC cells through miR-485-5p/MMP14 axis

Rescue experiments were conducted to assess whether circPTCH1 promotes RCC migration and invasion through the miR-485-5p/MMP14 axis. The results of wound healing and transwell assays were consistent with previous data that attenuation of circPTCH1 decreased the migration of RCC cells. However, this effect was partly abolished after co-transfection with miR-485-5p inhibitors (Figure 5A-C). Similarly, the invasive abilities of OS-RC-2 and A498 cells were reversed with simultaneous inhibition of miR-485-5p (Figure 5D). The biological role of MMP14 was also determined using siRNA to silence its expression. Consistent with a previous study [32], MMP14 silencing suppressed migration and invasion of RCC cells and alleviated the pro-migration and -invasion effect of circPTCH1 on RCC cells (Figure S5). In addition, knockdown of circPTCH1 decreased the protein level of MMP14, while co-transfection with the miR-485-5p inhibitor partially restored its expression (Figure 5G).

EMT has been known as an important phenotypic indicator for tumor invasion and metastasis, by which epithelial cells acquire molecular alterations that lose their epithelial characterizations and obtain a mesenchymal feature [33]. Here, we performed gene set enrichment analysis (GSEA) based on TCGA RCC dataset. As shown in Figure 5E, high MMP14 expression was associated with EMT (NES = 2.62; FDR < 0.01). Notably, morphological alterations of RCC cells were observed under light

microscopy. After up-regulating circPTCH1 levels, a greater fraction of RCC cells gained a spindly, fibroblast-like morphology, which was consistent with characteristics of EMT (Figure 5F). We also measured the expression of several EMT pathway-related genes by western blot analysis. As expected, in circPTCH1-knockdown RCC cells, the expression of epithelial marker E-cadherin was increased and mesenchymal markers, N-cadherin and vimentin, were decreased (Figure 5G). Similar findings were also obtained using immunofluorescence analysis (Figure 5H). Together, the results of Figure 5A-H reveal that circPTCH1 promotes RCC migration, invasion and EMT through regulation of miR-485-5p/MMP14 signaling.

circPTCH1 promotes tumor metastasis *in vivo*

To further confirm the effect of circPTCH1 on RCC metastasis *in vivo*, we constructed stable circPTCH1 over-expressing cell line by infecting OS-RC-2 cells with circPTCH1-overexpressed lentivirus. The cells had been previously transfected with firefly luciferase [9]. 1×10^6 cells (circPTCH1-Vector or OE-circPTCH1) were injected into each mouse under the left subrenal capsule. The role of miR-485-5p on RCC metastasis was also investigated through tail vein injection with agomir-485-5p or NC. The injection scheme presented in Figure 6A was designed according to previous research [25]. After 6 weeks, we found that mice in OE-circPTCH1 group developed more metastases compared with vector, and agomir-485-5p suppressed the progression of RCC and attenuated the effect of circPTCH1 (Figure 6B). The mice were then sacrificed and the total metastatic foci in lung, liver, colon, spleen and the contralateral kidney were counted using IVIS (Figure 6C-D). Elevated circPTCH1 expression led to an increased rate of metastasis as well as an increase in total metastatic foci and secondary metastatic lung tumor growth, while miR-485-5p inhibited this effect of circPTCH1 on RCC (Figure 6E-G). In parallel, IHC analysis was applied to detect MMP14, E-cadherin, and N-cadherin protein levels in tumor tissues from each group. Consistent with *in vitro* data, the expression of MMP14 and N-cadherin was up-regulated in the circPTCH1-OE group and down-regulated in the agomir-485-5p group, and the circPTCH1-induced increase in MMP14-EMT signaling was suppressed by injection of agomir-485-5p (Figure 6H). Taken together, these results indicate that circPTCH1 promotes RCC progression and metastasis via modulating miR-485-5p/MMP14/EMT signaling.

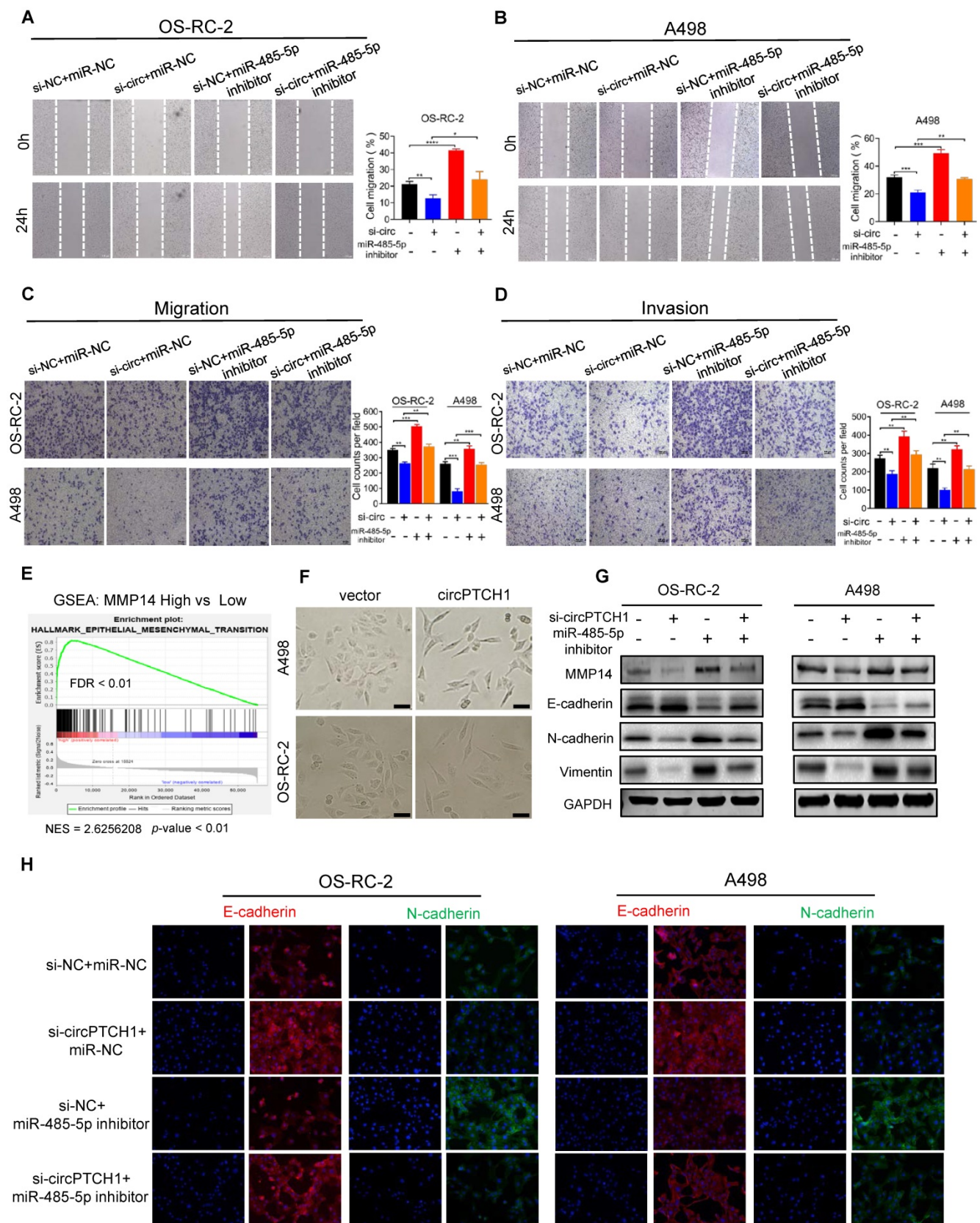


Figure 5. circPTCH1 facilitates migration, invasion and EMT of RCC cells through miR-485-5p/MMP14 axis. **A-D.** Wound healing and transwell assays showed the migration and invasion abilities of RCC cells after various treatments. **E.** GSEA analysis based on TCGA data showed that EMT was enriched in MMP14 overexpressed group. **F.** Bright field images of RCC cells morphology changes after overexpressing circPTCH1. Magnification $\times 100$. **G.** The expressions of MMP14, epithelial marker (E-cadherin) and mesenchymal markers (N-cadherin and Vimentin) were detected by western blot. **H.** The expressions of E-cadherin and N-cadherin were detected by immunofluorescence analysis. Scale bar, 100 μ m. * $p < 0.05$, ** $p < 0.01$, *** $p < 0.001$. **** $p < 0.0001$. NC: negative control; EMT: epithelial-mesenchymal transition; RCC: renal cell carcinoma. GSEA: gene set enrichment analysis.

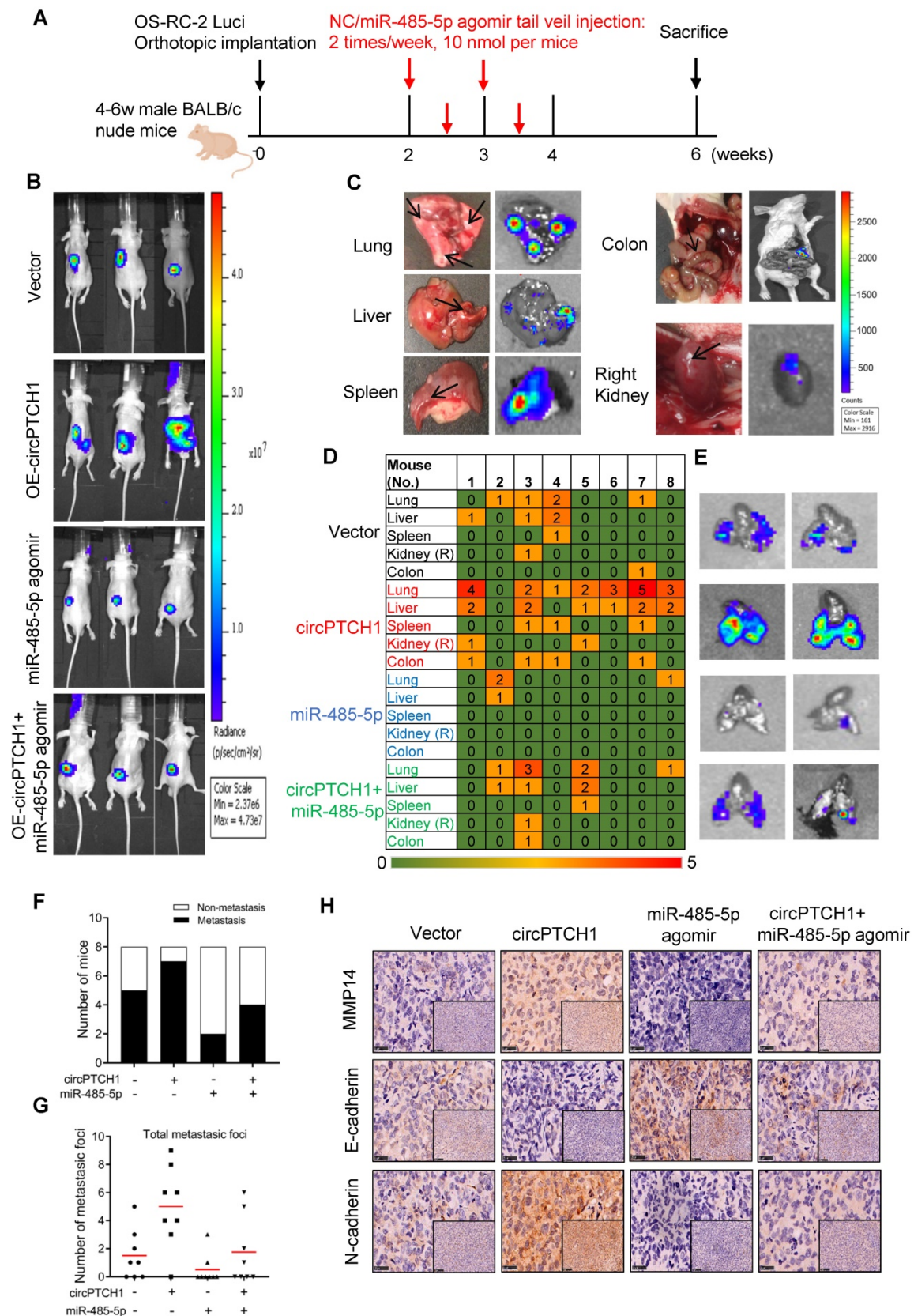


Figure 6. circPTCH1 promotes tumor metastasis in vivo. **A.** The flow diagram showed the scheme of tail vein injection with agomir miR-485-5p or NC into nude mice. **B.** IVIS imaging of mice 6 weeks after the orthotopically implant under the subrenal capsule of left kidney. Mice were distributed into 4 groups: vector, OE-circPTCH1, miR-485-5p agomir and OE-circPTCH1+miR-485-5p agomir (n = 8 each group). **C.** Representative photos and organ bioluminescent images of metastasis in lung, liver, colon, spleen, and the right kidney. **D.** Array diagram showed the metastatic status in various organs of each mouse in four groups. **E.** Representative bioluminescent images of lung metastases in four groups. **F.** Quantification of the metastasis rate in four groups. **G.** Total metastatic foci in each mouse of four groups. **H.** IHC detection of MMP14, E-cadherin and N-cadherin expression in tumor samples from nude mice in four groups. Magnification $\times 100$ and $\times 400$. NC: negative control; IHC: immunohistochemistry; IVIS: *in vivo* imaging system.

Table 1. The correlation between circPTCH1 level and various clinicopathologic features

Characteristics	Samples	circPTCH1 expression		P value
		Low	High	
Total	39	20	19	
Age				0.109
<60	22	11	11	
≥60	17	9	8	
Gender				0.504
Male	26	11	15	
Female	13	9	4	
T stage				0.118
1+2	33	18	15	
3+4	6	2	4	
Metastasis				0.032*
No	31	19	12	
Yes	8	1	7	
Fuhrman grade				0.045*
I+ II	30	18	12	
III+IV	9	2	7	

* Statistically significant.

Discussion

Numerous circRNAs have recently been identified with the development of high-throughput sequencing and advanced bioinformatics technology [34], and the relationship between circRNAs and cancers has drawn more attention than before. In this

study, we reported a novel circRNA (circBase ID: hsa_circ_0139402) generated from exons 13 and 14 of the PTCH1 gene and evaluated its effect on RCC progression and metastasis.

Although TKI and ICI drugs for metastatic RCC have been developed, the prognosis remains very poor, with a five-year survival rate less than 10% [2, 7]. Thus, there is a significant need to clarify the mechanism of metastasis in RCC. In this study, we elucidated a new mechanism that RCC may develop metastasis ascribed to the dysregulated circPTCH1/miR-485-5p/MMP14 signaling (Figure 7). Our study demonstrated that circPTCH1 was up-regulated in the microarray analysis, tumor cell lines and clinical RCC samples, and high circPTCH1 levels were positively correlated with the degree of malignancy in patients with RCC. Upregulation of circPTCH1 stimulated RCC migration and invasion both *in vitro* and *in vivo* whereas inhibiting circPTCH1 reduced migration and invasion of RCC cells. Given the stability of circRNAs, they may represent a promising new type of diagnostic biomarker for cancers in the future. In the present research, we did not measure circPTCH1 levels in peripheral blood or urine of RCC patients due to the lack of samples. However, further studies need performed to investigate the expression of

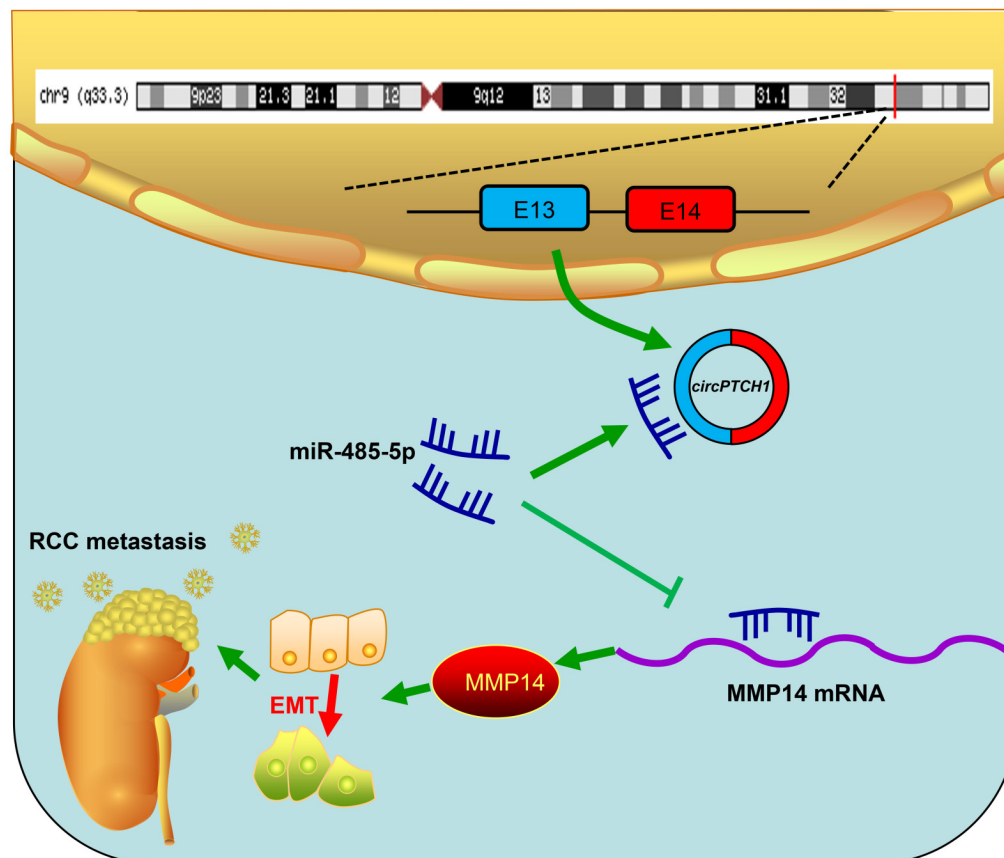


Figure 7. Schematic diagram illustrates that circPTCH1 promotes RCC metastasis through miR-485-5p/MMP14 axis. RCC: renal cell carcinoma; EMT: epithelial-mesenchymal transition; E: exon.

circPTCH1 in the circulation of RCC patients, which may indicate a newly and non-invasive method for RCC diagnosis.

Recently, circRNAs have been shown to be closely associated with tumorigenesis, such as cervical cancer [35], lung carcinoma [36], gastric cancer [37], hepatocellular carcinoma [38] and renal cell carcinoma. Xue *et al.* found that circ-AKT3 was lowly expressed in RCC tissues and suppressed the metastasis of RCC through activating the miR-296-3p/E-cadherin signaling pathway [39]. circ-RAPGEF5 was reported to inhibit the growth and metastasis of RCC via the miR-27a-3p/TXNIP axis [40]. circPRRC2A induces angiogenesis and metastasis through sponging miR-514a-5p and miR-6776-5p, and upregulating TRPM3 in RCC [41]. Most of the studies on circRNAs have focused on the mechanism by which circRNAs function as a sponge of miRNA, thus influencing the target gene level. However, this competing endogenous RNA (ceRNA) effect is dependent on the cytoplasmic localization of circRNA and cannot be generally applied [42]. It has been reported that circ-DONSON, which is mainly distributed in the nucleus, regulates the transcription of SOX4 by recruiting the NURF complex to its promoter [43], and circ-FBXW7, which is also located in the nucleus, represses glioma tumorigenesis through encoding a novel 21-kDa protein, FBXW7-185aa [44]. In the present study, circPTCH1 was predominantly localized to the cytoplasm and acts as a sponge to competitively bind with miR-485-5p as demonstrated through RNA pull-down, RIP and dual-luciferase reporter assays.

MiR-485-5p has already been reported to suppress the progression of several tumors such as hepatocellular carcinoma, colorectal cancer and non-small cell lung cancer [18, 29, 45]. However, its effect on RCC remained unknown. Here in this study, we firstly assessed the effect of miR-485-5p on RCC both *in vitro* and *in vivo*. The results demonstrate that miR-485-5p is aberrantly down-regulated in tumor specimens and could also suppress the migration and invasion of RCC cells.

MMP14 (also known as MT1-MMP), one of the zinc-dependent matrix metalloproteinase family, has been shown to promote EMT transition and induces invasive and metastatic activities in various tumors including RCC, through degrading extracellular matrix components (ECM) and several bioactive molecules [46-48]. In the present study, MMP14 was predicted as the target of miR-485-5p by several online databases. Notably, the interaction between miR-485-5p and MMP14 has been investigated in previous publications. Bo *et al.* reported that LncRNA-MFI2AS1 promotes the growth, migration,

and invasion of glioma cells by modulating MMP14 levels *via* miR-485-5p [31], and Cheng's study also implied that Lnc-UCA1 stimulates epithelial ovarian cancer through miR-485-5p/MMP14 signaling [49]. Here, the interaction between miR-485-5p and MMP14 was confirmed by luciferase reporter analysis in RCC cells. Moreover, we observed that miR-485-5p expression level was inversely correlated with MMP14 in RCC clinical samples and the MMP14 protein levels were affected by transfection with miR-485-5p mimics or inhibitors, supporting the hypothesis that miR-485-5p targets MMP14.

In the present study, we explored the expression and function of circPTCH1 in RCC. However, the role of its host gene PTCH1, remains uncertain until now. One paper detected the immunohistochemical expression of PTCH1 in 140 ccRCC specimens and found that PTCH1 is more highly expressed in G3/G4 than in G1/G2 tumors (1.5-fold, $p = 0.02$) [50], which was consistent with our findings of circPTCH1. Another study evaluated the expression of PTCH1 in 37 ccRCC tumor and control tissues, however, no statistically significant differences were observed [51]. Though circRNAs are typically described as having a similar function as their linear counterparts, antagonistic and independent functions of linear and circular RNA have also been reported previously. One study reported that circPOK functioned as a non-coding, proto-oncogenic RNA in mesenchymal tumors, in contrast to its linear gene Pokemon (functions as a tumor suppressor) [52]. To clarify the molecular mechanism behind this role, the authors proposed and verified several hypotheses: sponging for miRNAs; encoding new proteins; and regulating the functionality of RNA-binding proteins through direct binding. Inspired by this study, we will investigate the role of PTCH1 in RCC and explore the underlying mechanisms in our future work.

In summary, this study indicates that circPTCH1 is highly expressed in RCC cells and tissues, and promotes RCC progression and metastasis by modulating MMP14 expression and activating EMT process via sponging miR-485-5p. These findings reveal a novel signaling pathway that may be applied as a potential prognostic biomarker and therapeutic target in metastatic RCC.

Abbreviations

RCC: renal cell carcinoma; KIRC: kidney clear cell carcinoma; ncRNA: non-coding RNA; FC: fold change; circPTCH1: circular RNA PTCH1; EMT: epithelial-mesenchymal transition; IHC: immunohistochemistry; qRT-PCR: quantitative real-time PCR; TCGA: the cancer genome atlas; CPTAC: clinical

proteomic tumor analysis consortium; FISH: fluorescence *in situ* hybridization; RIP: RNA immunoprecipitation; siRNA: small-interfering RNA; WT: wild-type; MUT: mutant-type; PTCH1: patched 1; MMP14: matrix metalloproteinase 14; NC: negative control; DMEM: dulbecco's modified eagle's medium; FBS: fetal bovine serum; cDNA: complementary DNA; gDNA: genomic DNA; IVIS: *in vivo* imaging system.

Supplementary Material

Supplementary figures and tables.

<http://www.thno.org/v10p10791s1.pdf>

Acknowledgements

This study was supported by funding from the National Natural Science Foundation of China (No. 81370699, 81971371, 81902567 and 81972369) and The Shanghai Youth Talent Support Program (W. Zhai). The authors would also like to thank the grant from China Scholarship Council.

Author Contributions

HL, WZ and YX conceived and designed the study. HL and GH performed all the *in vitro* and *in vivo* experiments. WZ provided support with experimental techniques. HL and QL collected clinical data. ZW performed the pathologic analyzes. JZ and YC analyzed the data and prepared the manuscript. WZ reviewed and revised the manuscript. YH, WX, WZ and YX provided material support and supervised all experiments. All authors read and approved the final manuscript.

Ethics approval

This study was approved by the Ethics Committee of Shanghai Tenth People's Hospital of Tongji University and Renji Hospital of School of Medicine in Shanghai JiaoTong University. Written informed consent was obtained from all patients. All animal experiments were conducted according to the protocols of the Institutional Animal Care and Use Committee of Shanghai Tenth People's Hospital.

Competing Interests

The authors have declared that no competing interest exists.

References

- Siegel RL, Miller KD, Jemal A. Cancer statistics, 2020. *CA Cancer J Clin.* 2020; 70: 7-30.
- Patard JJ, Pignot G, Escudier B, Eisen T, Bex A, Sternberg C, et al. ICUD-EAU international consultation on kidney cancer 2010: treatment of metastatic disease. *Eur Urol.* 2011; 60: 684-90.
- Drangsholt S, Huang WC. Current trends in renal surgery and observation for small renal masses. *Urol Clin North Am.* 2017; 44: 169-78.
- Ljungberg B, Bensalah K, Canfield S, Dabestani S, Hofmann F, Hora M, et al. EAU guidelines on renal cell carcinoma: 2014 update. *Eur Urol.* 2015; 67: 913-24.
- Yin L, Gao S, Shi H, Wang K, Yang H, Peng B. TIP-B1 promotes kidney clear cell carcinoma growth and metastasis via EGFR/AKT signaling. *Aging.* 2019; 11: 7914-37.
- Touma NJ, Hosier GW, Di Lena MA, Leslie RJ, Ho L, Menard A, et al. Growth rates and outcomes of observed large renal masses. *Can Urol Assoc J.* 2018; 276-81.
- Albiges L, Powles T, Staehler M, Bensalah K, Giles RH, Hora M, et al. Updated european association of urology guidelines on renal cell carcinoma: immune checkpoint inhibition is the new backbone in first-line treatment of metastatic clear-cell renal cell carcinoma. *Eur Urol.* 2019; 76: 151-6.
- Van der Mijn JC, Mier JW, Broxterman HJ, Verheul HM. Predictive biomarkers in renal cell cancer: insights in drug resistance mechanisms. *Drug Resist Updat.* 2014; 17: 77-88.
- Gong D, Zhang J, Chen Y, Xu Y, Ma J, Hu G, et al. The m(6)A-suppressed P2RX6 activation promotes renal cancer cells migration and invasion through ATP-induced Ca(2+) influx modulating ERK1/2 phosphorylation and MMP9 signaling pathway. *J Exp Clin Cancer Res.* 2019; 38: 233.
- Chen LL, Yang L. Regulation of circRNA biogenesis. *RNA Biol.* 2015; 12: 381-8.
- Memczak S, Jens M, Elefsinioti A, Torti F, Krueger J, Rybak A, et al. Circular RNAs are a large class of animal RNAs with regulatory potency. *Nature.* 2013; 495: 333-8.
- Guarnerio J, Bezzi M, Jeong JC, Paffenholz SV, Berry K, Naldini MM, et al. Oncogenic role of fusion-circRNAs derived from cancer-associated chromosomal translocations. *Cell.* 2016; 166: 1055-6.
- Cocquerelle C, Mascrez B, Hetuin D, Bailluel B. Mis-splicing yields circular RNA molecules. *FASEB J.* 1993; 7: 155-60.
- Du WW, Yang W, Liu E, Yang Z, Dhaliwal P, Yang BB. Foxo3 circular RNA retards cell cycle progression via forming ternary complexes with p21 and CDK2. *Nucleic Acids Res.* 2016; 44: 2846-58.
- Zhen N, Gu S, Ma J, Zhu J, Yin M, Xu M, et al. CircHMGCS1 promotes hepatoblastoma cell proliferation by regulating the IGF signaling pathway and glutaminolysis. *Theranostics.* 2019; 9: 900-19.
- Xia X, Li X, Li F, Wu X, Zhang M, Zhou H, et al. A novel tumor suppressor protein encoded by circular AKT3 RNA inhibits glioblastoma tumorigenicity by competing with active phosphoinositide-dependent Kinase-1. *Mol Cancer.* 2019; 18: 131.
- Svoronos AA, Engelman DM, Slack FJ. OncomiR or tumor suppressor? the duplicity of microRNAs in cancer. *Cancer Res.* 2016; 76: 3666-70.
- Gao J, Dai C, Yu X, Yin XB, Zhou F. microRNA-485-5p inhibits the progression of hepatocellular carcinoma through blocking the WBP2/Wnt signaling pathway. *Cell Signal.* 2020; 66: 109466.
- Wang R, Zuo X, Wang K, Han Q, Zuo J, Ni H, et al. MicroRNA-485-5p attenuates cell proliferation in glioma by directly targeting paired box 3. *Am J Cancer Res.* 2018; 8: 2507-17.
- Mancuso M, Pazzaglia S, Tanori M, Hahn H, Merola P, Rebessi S, et al. Basal cell carcinoma and its development: insights from radiation-induced tumors in Ptc1-deficient mice. *Cancer Res.* 2004; 64: 934-41.
- Hasanovic A, Mus-Veteau I. Targeting the multidrug transporter ptc1 potentiates chemotherapy efficiency. *Cells.* 2018; 7.
- Chandrashekar DS, Bashel B, Balasubramanya SAH, Creighton CJ, Ponce-Rodriguez I, Chakravarthi B, et al. UALCAN: a portal for facilitating tumor subgroup gene expression and survival analyses. *Neoplasia (New York, NY).* 2017; 19: 649-58.
- Shi Y, Guo Z, Fang N, Jiang W, Fan Y, He Y, et al. hsa_circ_0006168 sponges miR-100 and regulates mTOR to promote the proliferation, migration and invasion of esophageal squamous cell carcinoma. *Biomed Pharmacother.* 2019; 117: 109151.
- Dong W, Bi J, Liu H, Yan D, He Q, Zhou Q, et al. Circular RNA ACVR2A suppresses bladder cancer cells proliferation and metastasis through miR-626/EYA4 axis. *Mol Cancer.* 2019; 18: 95.
- Zhou Y, Chen E, Tang Y, Mao J, Shen J, Zheng X, et al. miR-223 overexpression inhibits doxorubicin-induced autophagy by targeting FOXO3a and reverses chemoresistance in hepatocellular carcinoma cells. *Cell Death Dis.* 2019; 10: 843.
- Zhai W, Zhu R, Ma J, Gong D, Zhang H, Zhang J, et al. A positive feed-forward loop between LncRNA-URRCC and EGFL7/P-AKT/FOXO3 signaling promotes proliferation and metastasis of clear cell renal cell carcinoma. *Mol Cancer.* 2019; 18: 81.
- Chen LL. The biogenesis and emerging roles of circular RNAs. *Nat Rev Mol Cell Biol.* 2016; 17: 205-11.
- Wang Y, Sun L, Wang L, Liu Z, Li Q, Yao B, et al. Long non-coding RNA DSCR8 acts as a molecular sponge for miR-485-5p to activate Wnt/beta-catenin signal pathway in hepatocellular carcinoma. *Cell Death Dis.* 2018; 9: 851.
- Huang RS, Zheng YL, Li C, Ding C, Xu C, Zhao J. MicroRNA-485-5p suppresses growth and metastasis in non-small cell lung cancer cells by targeting IGF2BP2. *Life Sci.* 2018; 199: 104-11.
- Chen F, Chandrashekar DS, Varambally S, Creighton CJ. Pan-cancer molecular subtypes revealed by mass-spectrometry-based proteomic characterization of more than 500 human cancers. *Nat Commun.* 2019; 10: 5679.

31. Liu K, Liu J, Bo QF. MF12-AS1 regulates the aggressive phenotypes in glioma by modulating MMP14 *via* a positive feedback loop. *Eur Rev Med Pharmacol Sci.* 2019; 23: 5884-95.
32. Wan G, Liu Y, Zhu J, Guo L, Li C, Yang Y, *et al.* SLFN5 suppresses cancer cell migration and invasion by inhibiting MT1-MMP expression *via* AKT/GSK-3 β /beta-catenin pathway. *Cell Signal.* 2019; 59: 1-12.
33. Yeung KT, Yang J. Epithelial-mesenchymal transition in tumor metastasis. *Mol Oncol.* 2017; 11: 28-39.
34. Yu CY, Kuo HC. The emerging roles and functions of circular RNAs and their generation. *J Biomed Sci.* 2019; 26: 29.
35. Ji F, Du R, Chen T, Zhang M, Zhu Y, Luo X, *et al.* Circular RNA circSLC26A4 Accelerates Cervical Cancer Progression *via* miR-1287-5p/HOXA7 Axis. *Mol Ther Nucleic Acids.* 2019; 19: 413-20.
36. Cheng Z, Yu C, Cui S, Wang H, Jin H, Wang C, *et al.* circTP63 functions as a ceRNA to promote lung squamous cell carcinoma progression by upregulating FOXM1. *Nat Commun.* 2019; 10: 3200.
37. Lu J, Wang YH, Yoon C, Huang XY, Xu Y, Xie JW, *et al.* Circular RNA circ-RanGAP1 regulates VEGFA expression by targeting miR-877-3p to facilitate gastric cancer invasion and metastasis. *Cancer Lett.* 2020; 471: 38-48.
38. Zhu YJ, Zheng B, Luo GJ, Ma XK, Lu XY, Lin XM, *et al.* Circular RNAs negatively regulate cancer stem cells by physically binding FMRP against CCAR1 complex in hepatocellular carcinoma. *Theranostics.* 2019; 9: 3526-40.
39. Xue D, Wang H, Chen Y, Shen D, Lu J, Wang M, *et al.* Circ-AKT3 inhibits clear cell renal cell carcinoma metastasis *via* altering miR-296-3p/E-cadherin signals. *Mol Cancer.* 2019; 18: 151.
40. Chen Q, Liu T, Bao Y, Zhao T, Wang J, Wang H, *et al.* CircRNA cRAPGEF5 inhibits the growth and metastasis of renal cell carcinoma *via* the miR-27a-3p/TXNIP pathway. *Cancer Lett.* 2020; 469: 68-77.
41. Li W, Yang FQ, Sun CM, Huang JH, Zhang HM, Li X, *et al.* circPRRC2A promotes angiogenesis and metastasis through epithelial-mesenchymal transition and upregulates TRPM3 in renal cell carcinoma. *Theranostics.* 2020; 10: 4395-409.
42. Legnini I, Di Timoteo G, Rossi F, Morlando M, Briganti F, Sthandier O, *et al.* Circ-ZNF609 is a circular RNA that can be translated and functions in myogenesis. *Mol Cell.* 2017; 66: 22-37.e9.
43. Ding L, Zhao Y, Dang S, Wang Y, Li X, Yu X, *et al.* Circular RNA circ-DONSON facilitates gastric cancer growth and invasion *via* NURF complex dependent activation of transcription factor SOX4. *Mol Cancer.* 2019; 18: 45.
44. Yang Y, Gao X, Zhang M, Yan S, Sun C, Xiao F, *et al.* Novel role of FBXW7 circular RNA in repressing glioma tumorigenesis. *J Natl Cancer Inst.* 2018; 110: 304-15.
45. Hu XX, Xu XN, He BS, Sun HL, Xu T, Liu XX, *et al.* microRNA-485-5p functions as a tumor suppressor in colorectal cancer cells by targeting CD147. *J Cancer.* 2018; 9: 2603-11.
46. Cao J, Chiarelli C, Richman O, Zarrabi K, Kozarekar P, Zucker S. Membrane type 1 matrix metalloproteinase induces epithelial-to-mesenchymal transition in prostate cancer. *J Biol Chem.* 2008; 283: 6232-40.
47. Liu M, Qi Y, Zhao L, Chen D, Zhou Y, Zhou H, *et al.* Matrix metalloproteinase-14 induces epithelial-to-mesenchymal transition in synovial sarcoma. *Hum Pathol.* 2018; 80: 201-9.
48. Petrella BL, Brinckerhoff CE. Tumor cell invasion of von Hippel Lindau renal cell carcinoma cells is mediated by membrane type-1 matrix metalloproteinase. *Mol Cancer.* 2006; 5: 66.
49. Yang Y, Jiang Y, Wan Y, Zhang L, Qiu J, Zhou S, *et al.* UCA1 functions as a competing endogenous RNA to suppress epithelial ovarian cancer metastasis. *Tumour Biol.* 2016; 37: 10633-41.
50. Jäger W, Thomas C, Fazli L, Hurtado-Coll A, Li E, Janssen C, *et al.* DHH is an independent prognosticator of oncologic outcome of clear cell renal cell carcinoma. *J Urol.* 2014; 192: 1842-8.
51. Kotulak-Chrzaszcz A, Klacz J, Matuszewski M, Kmiec Z, Wierzbicki PM. Expression of the sonic hedgehog pathway components in clear cell renal cell carcinoma. *Oncol Lett.* 2019; 18: 5801-10.
52. Guarnerio J, Zhang Y, Cheloni G, Panella R, Mae Katon J, Simpson M, *et al.* Intragenic antagonistic roles of protein and circRNA in tumorigenesis. *Cell Res.* 2019; 29: 628-40.